Application of infiltrated LSCM-GDC oxide anode in direct carbon/coal fuel cells

Xiangling Yue [a]*, Ana Arenillas [b], and John T S Irvine [a]

[a] *School of chemistry, University of St Andrews, St Andrews, Fife KY16 9ST, UK*

[b] *Instituto Nacional del Carbon (CSIC), 33080 Oviedo, Spain*

Abstract

Hybrid direct carbon/coal fuel cells (HDCFCs) utilise an anode based upon a molten carbonate salt with an oxide conducting solid electrolyte for direct carbon/coal conversion. They can be fuelled by a wide range of carbon sources, and offer higher potential chemical to electrical energy conversion efficiency and potential to decrease CO_2 emissions compared to coal-fired power plants. In this study, the application of (La, Sr)(Cr, Mn)O_3 (LSCM) and (Gd, Ce)O_2 (GDC) oxide anode was explored in HDCFC system based on a running with two different carbons, an organic xerogel and a raw bituminous coal. The electrochemical performance of the HDCFC based on 1-2 mm thick 8 mol.% yttria stabilised zirconia (YSZ) electrolyte and the GDC-LSCM anode fabricated by wet impregnation procedures was characterized and discussed. The infiltrated oxide anode showed a significantly higher performance than the conventional Ni-YSZ anode, without suffering from impurity formation under HDCFC operation conditions. Total polarisation resistance (Rp) reached 0.8-0.9 Ω cm^2 from DCFC with oxide anode on xerogel and bituminous coal at 750ºC, with open circuit voltage (OCV) values in the range of 1.1-1.2V on both carbon forms. These indicated the potential application of LSCM-GDC oxide anode in HDCFCs. The chemical compatibility of LSCM/GDC with carbon/carbonate investigation revealed that the emergence of A_2BO_4 type oxide in replacement of ABO_3 perovskite structure in LSCM in reducing environment, due to Li attack as a result of intimate contact between LSCM and Li_2CO_3, with GDC being stable under identical conditions. Such reaction between LSCM and Li_2CO_3 was not observed on a LSCM-YSZ pellet treated with Li-K carbonate in 5% H_2/Ar at 700ºC, nor on GDC-LSCM anode after HDCFC operation. The HDCFC durability tests of GDC-LSCM oxide on xerogel and on raw bituminous coal were performed under potentiostatic operation at 0.7V at 750ºC. The degradation mechanisms were addressed, especially on the raw coal.

1. Introduction

With the ever increasing energy demands from human society, technologies have been developed concerning renewable resources utilization and energy efficiency enhancement for traditional fossil fuel sources, coupled with efforts to reduce CO_2 emissions. Amongst the different fuel cell technologies, direct carbon fuel cells (DCFCs) can be fuelled by a variety of carbon forms, such as

petroleum coke, coal, pyrolysed hydrocarbons and biomass etc., which is quite competitive to fuel cells based on gaseous fuels. By electrochemical oxidization of solid carbon to CO_2 product, a 100% thermodynamic efficiency can be obtained theoretically as a result of a nearly zero entropy change, DCFCs thus offer higher chemical to electrical energy conversion efficiency and lower level of CO_2 emissions due to ease for sequestration compared to traditional coal-fired power plants [1]. Furthermore, DCFCs provide high energy density by utilising solid carbon without intermediate reforming processes, compared to solid oxide fuel cells (SOFCs) that are powered by gaseous hydrocarbons [2]. These advantages make DCFC a very attractive technology.

Different types of DCFCs are in use depending on the electrolyte, for instance, molten carbonate [3-5], molten hydroxide [6], and solid oxide [7] etc. The hybrid DCFCs (HDCFCs) have gained increasing interest due to the benefits it brings [8]. The HDCFC utilises a binary electrolyte system, i.e. molten carbonate and solid oxide electrolyte, therefore, combines the molten carbonate fuel cell (MCFC) and solid oxide fuel cell technologies by mixing carbonate eutectic with solid carbon, with the resulting mixture supported on a solid electrolyte. Such a design simplifies the cell assembly on one hand, with solid electrolyte separating the cathode and anode compartments, reducing corrosion issues and eliminating CO_2 circulation/management encountered in MCFCs. It enhances the interactions between solid fuel and electrolyte, by extending the active reaction zone from a two-dimensional anode/solid electrolyte interface to three-dimensional slurry on the other hand, thus promotes the DCFC performance remarkably. Despite the prospects it offers, HDCFC faces a number of challenges due to the complexity in its system. So far, literature on this technology regarding anode materials, anode reaction mechanisms, performance stability, and proper fuels is limited.

Attempts have been made in our lab to solve some problems mentioned above [9-11]. A high DCFC power output that is comparable to a commercial SOFC was demonstrated [12]. Also a range of carbon forms including graphite, activated carbon, coals at different ranks and pine charcoal were tested in HDCFC, in an effort to link the carbon properties to fuel cell performance and stability [13]. Nonetheless, in all these studies, the anode material applied in for DCFC operation was restricted to the conventional Ni-YSZ cermet, which is subjected to several drawbacks that have been found in the development of SOFCs, such as sintering, poor redox stability and low tolerance to coke deposition and sulphur contaminations [14]. Indeed, Ni/NiO equilibrium was found to govern the anode reaction in HDCFC when carbon activity was low, giving a low open circuit voltage (OCV) and decreased thermodynamics [13]. The occurrence of Ni/NiO equilibration can also pose problems to mechanical integrity in SOFC owing to the volume expansion when Ni was oxidized, resulting in

failure in long term operation. Moreover, the endurance to sulphur poisoning is a significant concern when Ni-cermet is employed as most inexpensive and readily available coals/biomass contain sulphur impurity. Alternative anode materials that can be applied in HDCFC need to be searched for therefore.

(La, Sr)(Cr, Mn)O_3 (LSCM) perovskite-type material has been reported as an alternative anode in SOFCs, originated from its good redox stability, flexibility in fuel gas options and excellent resistance to coking and sulphur poisoning [15-16]. Other options include doped ceria, e.g. gadolinium doped ceria (GDC), which offers excellent electrochemical activity towards a series of oxidation/reduction reactions [17-18]. Previously, a GDC-LSCM electrode derived from wet-impregnation fabrication was demonstrated to have competitive performance to a well-behaved Ni-YSZ cermet in CO_2 electrochemical reduction in solid oxide electrolyser [19]. In the present work, GDC-LSCM oxides has been applied in HDCFC with its electrochemical performance towards carbon oxidation evaluated and its chemical stability in carbon-molten carbonate environment investigated. The carbon fuel studied covers organic xerogel, a synthetic carbon form from a sol-gel processing of resorcinol and formaldehyde under controlled conditions, as well as a bituminous coal. Besides, the electrochemical stability of GDC-LSCM oxide anode with carbonate has been examined after the durability of HDCFC operation on xerogel as well as on bituminous coal, with degradation mechanisms proposed.

2. Experimental

2.1 SOFC base fabrication

SOFCs with GDC impregnated LSCM-YSZ (abbreviated as GDC-LSCM hereinafter) anode and $(La_{0.8}Sr_{0.2})_{0.95}MnO_3$ (LSM)/YSZ//LSM cathode were prepared, details of which were described previously [19]. Briefly, these cells were based on an YSZ electrolyte (1mm or 2mm thick) supported structure with a two electrode geometry. YSZ powder (Pi-KEM) were pressed and fired to form a dense pellet, after which, a porous YSZ layer followed by a porous LSCM ($(La_{0.75}Sr_{0.25})_{0.97}Cr_{0.5}Mn_{0.5}O_3$, EMPA) layer were screen-printed on one side of YSZ pellet and fired at 1300^{o}C. Subsequently, a composite LSM/YSZ (50/50 by weight) layer followed by a pure LSM layer were introduced on the other side of dense YSZ pellet by screen-printing and sintered at 1100^{o}C. The following was the wet impregnation of gadolinium and cerium nitrate precursor solution, mixed according to the stoichiometric ratio of $Gd_{0.1}Ce_{0.9}O_2$, into the porous LSCM-YSZ backbone under a vacuum pressure of 0.15bar and thermal treatment at 500^{o}C to decompose nitrate

salts. The impregnation was repeated until a desirable loading amount of GDC, 50 wt. % over LSCM-YSZ, was reached. The resulting anode was then sintered at 1100^{o}C.

As comparison, an SOFC having Ni/YSZ anode was fabricated by screen printing anode and cathode ink at each side of YSZ pellet. The anode ink had NiO/YSZ in the ratio of 65/35 and the cathode ink was the same as in preparation of the SOFC with GDC-LSCM anode. The calcination temperature for Ni/YSZ anode and LSM/YSZ//LSM cathode were 1350^{o}C and 1100^{o}C respectively. A symmetric cell with LSM/YSZ//LSM introduced at both sides of YSZ pellet was prepared and measured in air at 650-800^{o}C to determine the cathode polarization contribution to total cell resistance, result shown in Table I. Prior to electrochemical characterization, Ag wires coated with Ag paste were attached to SOFCs as current collector and connections to electrochemical instrument.

Table I. Resistance from LSM/YSZ//LSM electrode in a symmetric cell in static air at 650-800^{o}C

	Operation temperature (^{o}C)				
	650	675	700	750	800
Rp (Ω cm^2)	1.68	1.12	0.81	0.41	0.22

2.2 DCFC testing and post-mortem analysis

The as-prepared SOFC was attached to the end of an alumina tube using ceramic adhesive (Aremco552), with the alumina tube acting as anode chamber sitting vertically in a temperature-programmed furnace. The solid fuel was placed inside the anode chamber at room temperature, with the fuel physically located on top of the SOFC anode. The furnace was heated to ~300^{o}C slowly to have ceramic adhesive properly cured firstly before ramping up to operational temperature, 650-750^{o}C (some cells were tested up to 800^{o}C). The cell was tested in a heating mode, in other words, it was measured at 650^{o}C and then at 700 and 750 or 800^{o}C respectively. At each temperature, the cell was stabilised until a steady OCV value was achieved before electrochemical testing.

Polarization curves and electrochemical impedance spectroscopy (EIS) were recorded for initial cell performance evaluation. For the former, the current density was recorded while sweeping cell potential from OCV value to –0.3V in 3mins. As for EIS, the impedance spectra were recorded in a frequency range from 150 KHz (stated otherwise) to 1Hz with a ac amplitude of 10mV using a potentiostat (Solartron1470) at OCV or at a certain current density (galvanostatic mode). After initial performance assessment, a stability measurement was conducted at 750^{o}C under potentiostatic mode (0.7V), with current density variation recorded as a function of operation time. In the course of electrochemical testing, the cathode was exposed to static air with the anode chamber being flushed

by a N_2 purge gas at a flow rate of 20ml/min. The N_2 gas was introduced by an alumina tube inserted into the anode chamber, with the end of the alumina tube at a small distance to the top of the pile of solid fuel. The exhaust gas from anode was carried by N_2 to an online gas chromatograph (GC) for composition analysis. For the symmetric cell, impedance spectra were measured under OCV at 650-800^oC with both electrodes exposed to static air.

After electrochemical characterization, the HDCFC anode was examined by a Panalytical X-ray diffractometer with Cu Kα radiation. The X-ray diffraction (XRD) was recorded in a two theta range 10-90^o at room temperature. The anode/cathode microstructure was inspected by scanning electron microscopy (SEM) using JSM 5600, coupled with Inca 2000 for energy dispersive X-ray spectroscopy (EDX) measurement.

2.3 Solid fuel characterizations and preparation

The solid fuels studied here included organic xerogel and a mineral bituminous coal (denoted as B-II-M), both supplied by INCAR-CSIC, Spain. Organic xerogel was synthesized by the sol-gel condensation of resorcinol (R) with formaldehyde (F) in deionised water followed by a vacuum evaporative drying process. The pH value of the precursor solution was controlled at 4 using Na_2CO_3 as the basification agent, and the R/F molar ratio was equal to the stoichiometric value (0.5), with the dilution ratio, D (the total solvent/reactant molar ratio) fixed at 5.7 during gel synthesis. Detailed synthesis procedures can be found elsewhere [20-21]. After drying, the resulting xerogel was sieved under 75μm for usage without any further treatments. With regard to coal sample, raw B-II-M coal was simply dry-milled in a bench mortar mill and sieved under 75microns, without any other processing. Table II (a) shows the chemical composition of the as-supplied xerogel and B-II-M samples. The chemical composition of carbon xerogel, obtained after pyrolysis of as-received organic xerogel at 700^oC in N_2 (described in detail in part 2.4) was also included in Table II (a). The standard used for sample composition analysis are as following: ASTM D-5373 in a LECO CHN 2000 for C, H, and N element, ASTM D-4239 for oxygen and sulphur in a LECO TRUSPEC Micro-O and LECO S632 respectively, ASTM 7582 for moisture and ash with ISO 562 for volatile matter in a LECO TGA-601 apparatus. Ash composition of the raw bituminous coal was also analysed using X-ray fluorescence in a Bruker SRS 3000, and the results is shown in Table II (b).

Table II. Chemical composition of xerogel and raw B-II-M coal (a), the ash content of B-II-M coal (b) as well as texture properties of organic xerogel (c)

(a)

Carbon type	Ultimate Analysis (wt%, dry ash free basis) C	H	N	O	S	Proximate Analysis (wt%, [a] dry basis) [a]FC	[a]VM	[a]Ash	Moisture	ΔH (kca/kg)
Organic xerogel	64.0	3.9	0.2	31.9	0.0	53.6	46.4	0.0	13.1	5862
Carbon xerogel	97.1	1.0	0.1	1.8	0.0	96.4	0.9	0.0	2.7	7762
B-II-M	90.4	4.6	1.5	2.8	0.7	73.9	19.4	6.7	0.7	5268

(b)

B-II-M ash composition (%)								
Fe_2O_3	Na_2O	MgO	Al_2O_3	SiO_2	P_2O_5	K_2O	CaO	TiO_2
11.9	0.9	2.0	20.0	35.5	0.0	2.6	14.0	1.1

(c)

	S_{BET} ($m^2\ g^{-1}$)	V_{micro} ($cm^3\ g^{-1}$)	Vmeso ($cm^3\ g^{-1}$)	Vmacro ($cm^3\ g^{-1}$)	d_{pore} (nm)
Organic xerogel	98	0.04	0.33	0.73	60

The pore texture of organic xerogel was measured by N_2 adsorption-desorption isotherms at -196°C using a Sorptomatic Carlo Erba 1900 device. The analysis of N_2 isotherms gave the BET specific surface area, S_{BET}; the micropore volume calculated by the Dubinin-Radushkevich Equation, V_{micro}. The mesopore volume (Vmeso), macropore volume (Vmacro) and the mean pore diameter (d_{pore}) were determined by mercury porosimetry with a Carlo Erba Porosimeter 2000. The textural properties of organic xerogel are provided in Table II (c).

Regarding fuel preparation for HDCFCs, the as–supplied xerogel/coal was pre-mixed with Li_2CO_3-K_2CO_3 carbonates (Li: K at a molar ratio of 62:38) by ball milling, at a weight ratio of carbon: carbonate 4:1, before loading into DCFC anode chamber. This was believed to give a homogeneous dispersion of xerogel/coal in Li_2CO_3-K_2CO_3 eutectic at operational temperature, thus to improve contacts and enhance the electrochemical oxidation of carbon. 2g of carbon/carbonates mixture was used for each test, with the fuel cell operated in a battery mode. After fuel cell testing, the remaining fuel was collected with its crystalline structure determined by XRD.

2.4 Compatibility of solid fuel, carbonates and SOFC anode components

The chemical compatibility between LSCM/GDC and carbon/carbonate mixture was examined. This involved the treatment of pre-mixed LSCM or GDC and carbon/carbonates powders at 700-800°C in N_2 or 5%H_2/Ar atmosphere and the identification of phases in residual powder after treatment. Organic xerogel and Li-K carbonates were mixed similarly to the preparation of solid fuel for electrochemical test, then LSCM or GDC powder was added with a weight ratio of 1:2 to carbonate

and ground for ~10min with a pestle and mortar. The above prepared powder mixture were placed in a crucible and thermally treated using a tube furnace. The furnace was heated to 150^{o}C and dwelled for 1 hour to remove moist, then it was heated to 700-800^{o}C and kept for 1 hour before cooling down to room temperature for XRD measurement. In this whole process, N_2 (otherwise, 5% H_2/Ar) at a flow rate of 20ml/min was flowing through the tube furnace. The xerogel/carbonate mixture was subjected to pyrolysis during this treatment.

In addition, a LSCM-YSZ pellet was prepared and treated. LSCM and YSZ powder in a ratio of 50:50 were mixed, pressed into pellet and fired at 1300^{o}C. The as-prepared pellet was immersed in Li_2CO_3-K_2CO_3 (at a molar ratio 62:38) mixture powder in an alumina crucible. The crucible was transferred into a tube furnace and heated to 700^{o}C in 5% H_2/Ar flow. The sample was kept at 700^{o}C for 10hrs before cooling down. This treatment was intended to mimic the conditions in HDCFC operation, where carbonate was contacting SOFC anode in a reducing environment. The LSCM-YSZ pellet was retrieved from molten salts at room temperature and measured by XRD for phase analysis, in comparison to a fresh LSCM-YSZ pellet.

3. Results and discussion

3.1 Fuel cell performance on different carbons

3.1.1 DCFC performance on organic xerogel and properties/characterizations of xerogel

Fig.1 shows the electrochemical performance of the HDCFC with GDC-LSCM SOFC anode operating on xerogel with N_2 as purge gas. The operation was conducted in a heating mode, i.e. the cell was tested stepwise from 650 to 750^{o}C. The purpose was to reduce the loss of carbon by chemical reaction due to Boudouard reaction (Equation 1) and decomposition of carbonate (Equation 2) which becomes much faster at high temperatures.

$$C + CO_2 \rightarrow 2CO \qquad \text{(Equation 1)}$$

$$CO_3^{2-} \rightarrow CO_2 + O^{2-} \qquad \text{(Equation 2)}$$

In Fig. 1(a), a fairly linear dependence of cell voltage on current density can be seen over the whole operation temperature range, with cell potential dropping slightly quicker at high current densities. With a 2mm thick YSZ electrolyte support, the power output for the HDCFC running with xerogel is nearly 45mW cm^{-2} at 750^{o}C. However, a total Rp value of ~0.8 Ω cm^2 and the cell area specific resistance (ASR) of ~5.3 Ω cm^2 are obtained in the impedance spectra in Fig. 1(b) at 750^{o}C. The ohmic resistance Rs, mainly from the thick YSZ electrolyte, takes up to 82% of the total cell

resistance (ASR). Therefore, one can expect much higher current density and power output if the electrolyte was made much thinner.

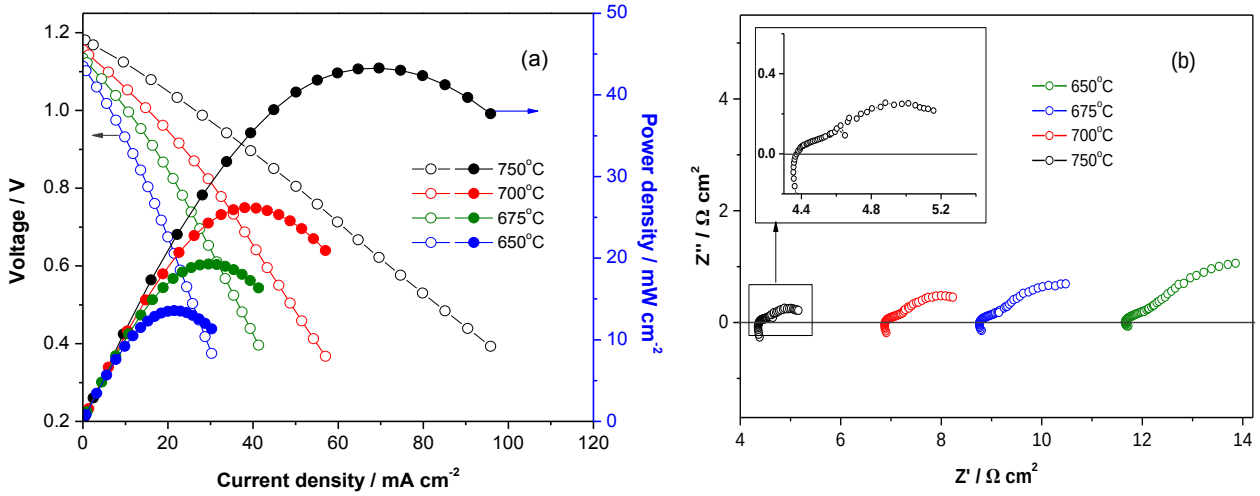

Fig.1 Current density-voltage and current density-power density (I-V and I-P) curves (a) and impedance spectra (b) of the DCFC with the GDC-LSCM SOFC anode operating at 650-750°C on xerogel. Note that the SOFC has a 2mm thick YSZ electrolyte and a LSM/YSZ//LSM cathode. The inset in impedance spectra is a zoom in the impedance spectrum at 750°C under OCV condition.

In Fig. 1(b), two semi-circular arcs are observed from the impedance spectra under OCV at different temperatures, with a small one at high frequency regime (10^4-10^3 Hz) and a dominant one at low frequency region with a characteristic frequency lower than 10 Hz. As temperature decreases, the cell resistance increases, with the low frequency contribution being affected more significantly. The characteristic frequency for the low frequency arc shifts to an even lower value (< 1Hz) at 650°C, while the value for high frequency arc stays unchanged compared to that at high temperature. The relevant processes for the above high frequency and low frequency arc are likely to be the charge transfer at the electrode-electrolyte interface and the mass transportations, respectively. Therefore, mass transfers become controlling processes, due to lowered thermodynamics and electrode kinetic as temperature drops.

The OCV value increases when operation temperature is raised in Fig. 1 (a), and it reaches 1.11, 1.16, and 1.18V at 650, 700 and 750°C respectively for DCFC with oxide anode. These values are higher than one can expect if the oxidation of carbon to carbon dioxide (Equation 3) occurred, for which the theoretical value is 1.02V.

$$C(g) + 2O^{2-} = CO_2\,(g) + 4e^- \qquad \text{(Equation 3)}$$

$$H_2(g) + O^{2-} = H_2O\ (g) + 2e^- \quad \text{(Equation 4)}$$

$$H_2(g) + CO_3^{2-} = CO_2(g) + H_2O(g) + 2e^- \quad \text{(Equation 5)}$$

Other reactions such as oxidation of H_2 (Equation 4-5) or hydrocarbons are therefore supposed to contribute to the higher OCV value. At 650°C, a theoretical OCV value of 1.12V is expected for a fuel cell supplied with humidified H_2 to anode and air to cathode. A GC analysis, performed to monitor HDCFC anode outlet gas during heating up, revealed H_2 evolution at temperature higher than 550°C with H_2 concentration reaching a peak at 700°C. However, H_2 alone cannot explain the high OCV at high temperatures such as 750°C, as the OCV for H_2 oxidation is anticipated to decrease against temperature. The decomposition of carbonate (Equation 2) was reported to impact OCV of HDCFC significantly, which was evidenced by adding 40mol% of Li_2O to carbon/carbonate slurry and demonstration of OCV values in the range of 1.2-1.3V at 550-700°C [10].

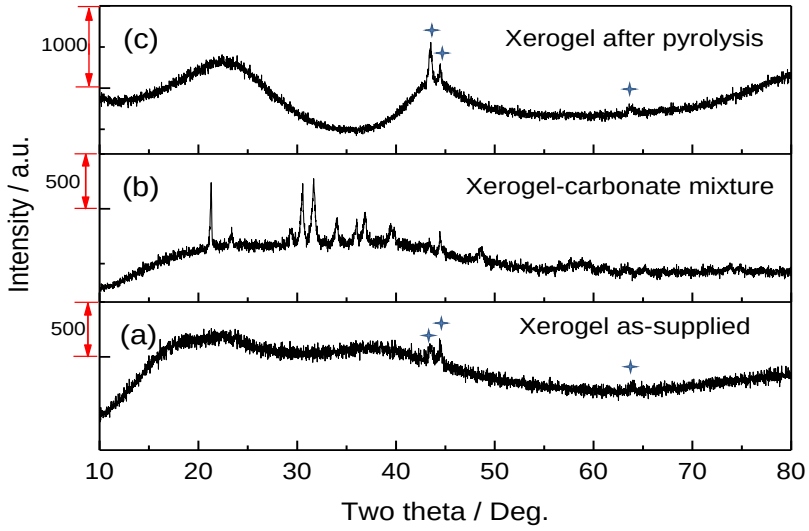

Fig. 2 XRD patterns of xerogel and xerogel-carbonate mixture: (a) as-supplied xerogel, (b) xerogel-carbonate power as-mixed, and (c) xerogel after pyrolysed at 700°C in N_2 without premixing with carbonate. Note that the cross labelled peaks are from sample holder.

Additionally, the high activity of xerogel towards oxidation cannot be ruled out for the observed high OCV values. The synthetic xerogel has a unique structure and its textural properties can be tuned to specific applications [21-22]. It possesses high surface area, high pore volume and a wide range of pore size, shown in Table II (c). The XRD diffraction patterns of as-supplied xerogel and as-mixed xerogel-carbonate mixture are presented in Fig. 2 (a-b). As one can see, a very broad feature of diffraction appears in two theta range of 10-50° for xerogel as well as xerogel/carbonate mixture. According to literature, the peak at 2θ = 20-30° can be ascribed to (002) reflection with the one at 2θ

= 40-50^o to (100) reflection for carbon materials [3-4]. These two peaks are very broad in the XRD pattern of xerogel sample, indicating a very disordered structure that is beneficial for carbon oxidation in DCFC. It has been agreed by several researchers that less crystalline carbon tends to have more edges sites and defects which are considered reactive sites for carbon oxidation in DCFC [3-4, 13]. One may argue that xerogel has quite low fixed carbon (53.6%) and a very high amount of volatile matter (46.4%), both of which were believed to impact DCFC performance negatively [13]. It should be pointed out that a carbonization process took place readily during heating up fuel cell to operational temperature, which changed the carbon chemical composition considerably. This was generally neglected in previous publications. The chemical composition of xerogel after pyrolysis (carbonization) in N_2 at 700^{o}C is compared to fresh xerogel in table II (a). Apparently, the fixed carbon ratio thus the calorific value (ΔH) is markedly promoted, with most volatile matter and moisture removed after carbonization. Despite the alteration in chemical composition, two well separated broad diffraction peaks at 2θ = 24^o and 2θ =44^o respectively are seen in xerogel after pyrolysis at 700^{o}C, as shown in Fig. 2(c), suggesting that low crystallinity and consequently high activity in xerogel remains after carbonization.

Illustrated in Fig.3 are the electrochemical performance of the HDCFC with a Ni-YSZ anode operated with xerogel at 700-800^{o}C. Similar OCV values (1.1-1.2V) are achieved compared to the cell with fully oxide anode. In Fig. 3(a), the I-V curves from the cell with Ni-YSZ SOFC anode are subjected to a curvature in the region where current density is low, due to high activation polarization losses. As current density increases, the cell is gradually controlled by ohmic polarization losses. In contrast, the I-V curves from the GDC-LSCM anode cell are almost linear in the whole measured current density range. These are supported by the declined Rp value and the depressed impedance arc in Fig. 3(c) from Ni-YSZ anode cell against increasing current density, whereas identical Rp values are attained upon drawing current up to 10mA at 750^{o}C on fully oxide anode cell (not shown here).

With the same configuration, DCFC with the Ni-YSZ anode has a maximum power density of only 30mW cm^{-2} at 800^{o}C, much lower than that from the GDC-LSCM anode cell at 750^{o}C. This observation is supported by the impedance comparison in Fig. 3(b) and Fig. 1(b). At 750^{o}C, the cell with Ni-YSZ anode exhibits an Rs of 5 Ωcm^2 and an ASR larger than 35 Ωcm^2. The appreciably high polarization resistance from Ni-YSZ anode cell implies a poor electro-catalytic activity from Ni-YSZ cermet towards carbon oxidation and retarded electrochemical reaction processes taking place on anode, in comparison to the anode composed of GDC-LSCM oxides. Furthermore, the Rs value takes up only 10-14% of the total cell resistance with respect to the cermet anode cell, a much

smaller portion than in the case when oxide anode is applied. This means that diminishing the solid electrolyte thickness is less likely to boost the cell performance tremendously in the cell with Ni-YSZ SOFC anode.

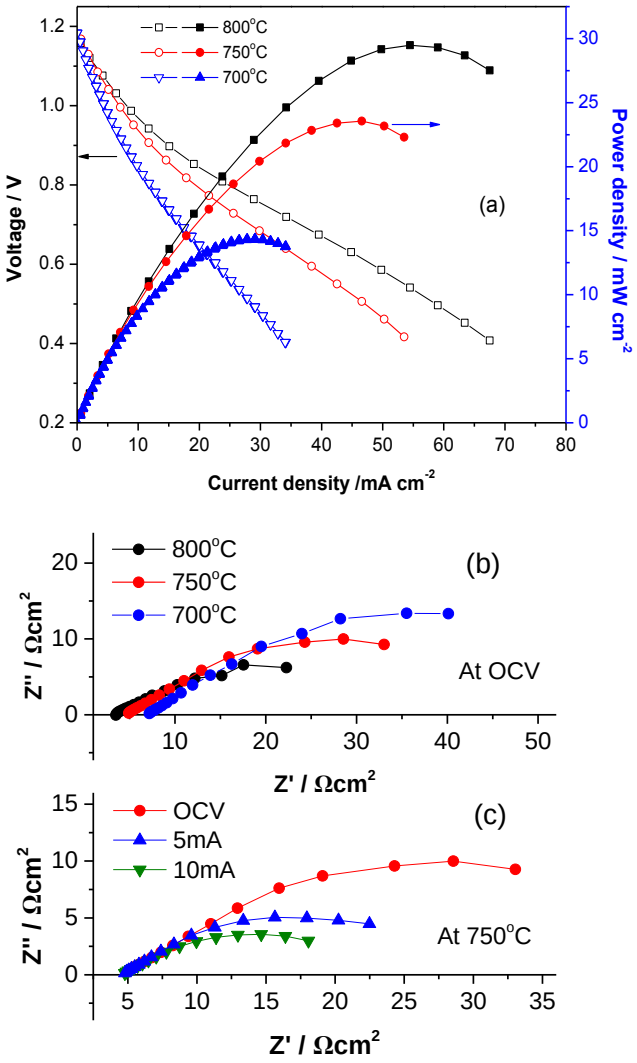

Fig.3 I-V and I-P curves (a) and impedance spectra at OCV (b) as well as at different current density at 750°C (c) of the HDCFC with a Ni-YSZ anode tested at 700-800°C on xerogel. Note that the SOFC have an identical structure to that with GDC-LSCM anode except the anode material.

The enhanced performance from the DCFC with a GDC-LSCM SOFC anode is probably attributed to the high ionic conductivity and electro-catalytic activity the oxide anode offers. GDC is a well-known oxide ion conductor, especially at temperature below 800°C. Besides, it offers mixed electronic and ionic conductivity in reducing atmosphere, which is beneficial for facile charge transfers and surface mass diffusions compared to the electrode has dual phases with separate electronic and ionic conductivity, for instance, Ni-YSZ cermet. It was reported by some researchers

that the conductivity and/or electro-catalytic activity was further reinforced when the active phase had a particle size down to nano scale [23], as encountered in the oxide anode. The wet impregnation-derived anode features a microstructure having fine GDC particles highly dispersed on the surface of LSCM support in the outer region and of YSZ substrate in the inner side of SOFC anode, which is believed to offer an extended active reaction zone as well as enhanced electro-catalytic properties towards electrode reactions.

3.1.2 DCFC performance on bituminous coal

It is desirable to utilise raw coal directly in DCFCs due to the abundance and low cost of this carbon source, however, it is quite challenging to run coal directly in DCFCs not only because of the poor knowledge on the links of physicochemical properties of coal to fuel cell performance, but also because of the impurities such as sulphur as well as ash contents in coal which might negatively influence DCFC long-term performance. Attempts have been made to correlate the chemical composition of coals with fuel cell performance, and tune the coal properties to promote DCFC performance by demineralization [5]. However, these require extra processing and cost. Alternatively, searching for catalyst or anode materials that are robust and durable in the harsh conditions subjected to the use of raw coals is necessary. Here the electrochemical results of a DCFC with GDC-LSCM oxides as SOFC anode utilising bituminous raw coal will be discussed.

The as-supplied B-II-M coal was mixed with Li_2CO_3-K_2CO_3 to serve as fuel, in the same manner as in xerogel. A 1mm thick YSZ pellet was applied as solid electrolyte with infiltration-derived GDC-LSCM oxide as SOFC anode. Fig. 4(a) presents the polarization behaviour and power output of the HDCFC operated on B-II-M coal in a heating mode. A linear response of cell voltage against current density is indicated in Fig. 4(a) in the whole potential range being measured. A maximum power density in excess of 60mW cm^{-2} is reached on raw coal at 750ºC. The power output is again limited by ohmic loss from the thick YSZ electrolyte, as seen from impedance results in Fig. 4(b). At 750ºC, an ASR value of ~4.2 Ω cm^2 is attained with Rs taking up a portion of 79% of total cell resistance on HDCFC with 1mm thick YSZ electrolyte and oxide anode running on raw bituminous coal.

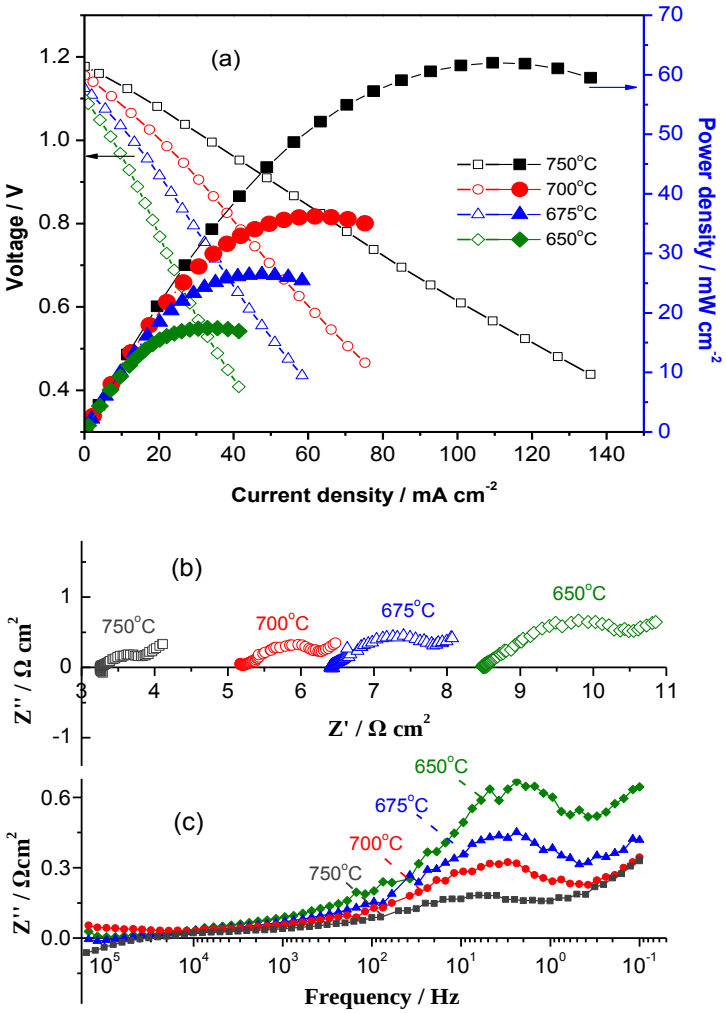

Fig. 4 (a) I-V, I-P curves and (b) complex impedance as well as (c) Bode impedance spectra of the HDCFC with 1mm thick YSZ solid oxide electrolyte and the GDC-LSCM oxide anode running on B-II-M coal at 650-750ºC.

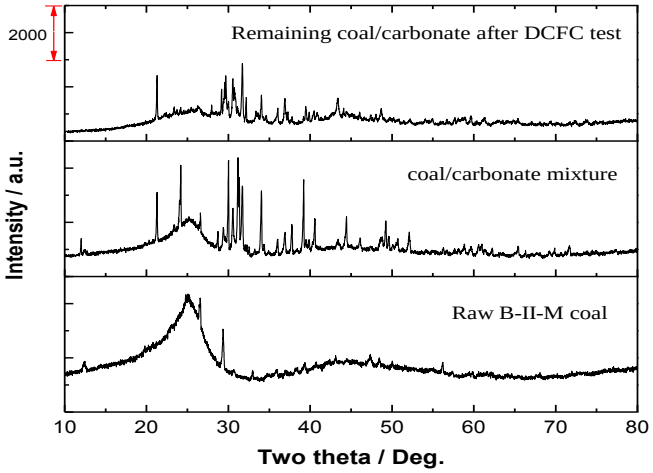

Fig. 5 XRD patterns of B-II-M raw coal and coal/carbonate mixtures before and after fuel cell testing.

On raw B-II-M coal, OCV values in the range of 1.1-1.18 are achieved at 650-750^{o}C, and the higher the temperature, the higher the OCV value, a similar trend as on xerogel. As H ratio is even higher in B-II-M coal (Table II (a)), the electrochemical oxidation reactions involved H_2 released from coal (Equation 4-5) may play a more important role in boosting OCV at the initial stage, especially at low temperatures. Besides, a low graphitic structure is also seen in the XRD pattern of B-II-M coal in Fig. 5, in which a broad peak appearing at $2\theta = 25.2^{o}$ and another weak and broaden feature at $2\theta = 35\text{-}55^{o}$ are indicated on this raw coal, apart from peaks due to mineral contents such as quartz.

In addition to the high OCV value, a total Rp ~0.9 Ω cm^2 at the lowest frequency in the impedance spectra is obtained from GDC-LSCM oxide on bituminous coal at 750^{o}C (Fig.4 (b)). The comparable Rp to that achieved on xerogel demonstrates that the GDC-LSCM oxide anode also performs greatly on raw B-II-M coal despite the existence of mineral matter and sulphur impurity. The complex impedance in Fig. 4(b) reveals a depressed arc followed by a spike at low frequency end at all temperature measured, and a characteristic frequency around 3Hz associated with the depressed arc is seen in the Bode impedance in Fig. 4(c). These suggest the limiting process for oxidation of coal on GDC-LSCM anode is associated with the diffusion of reactant to active sites.

3.2 Compatibility study of SOFC anode component with carbon/carbonate mixture

The compatibility of SOFC anode components with carbon/carbonates mixture is crucial for fuel cell performance and its long-term durability. The stability of LSCM and GDC with Li_2CO_3-K_2CO_3 in the atmosphere associated with the appearance of carbon was investigated in similar conditions as in DCFC operation but without the involvement of electrochemical reactions. Fig. 6 exhibits the room temperature XRD patterns of xerogel/carbonate/LSCM mixture after treated at 700-800^{o}C in different environments. Apparently, a typical ABO_3 perovskite structure is observed in LSCM after pyrolysis of xerogel-LSCM mixture at 800^{o}C in the absence of carbonate (Fig. 6(a)). However, diffraction peaks that can be assigned to a perovskite-related A_2BO_4 structure are identified from the xerogel-carbonate-LSCM mixture after treatment under the same conditions, besides the XRD peaks originated from Li$_2$CO3, $KHCO_3$ and other K-containing compounds (Fig. 6(c)). The A_2BO_4-type oxide has the K_2NiF_4 structure which is made up of the ABO_3 perovskite layer and an AO rock salt layer arranged one upon the other. On the other hand, the ABO_3 type perovskite structure is retained in LSCM after being treated with Li-K carbonate at 800^{o}C in the absence of carbon (Fig. 6(b)), implying that the reduction of ABO_3-type LSCM to A_2BO_4 is occurring only at the existence of carbon in the sample which brings a reductive treatment. As a confirmation, the XRD result of the Li_2CO_3-K_2CO_3-LSCM mixture subjected to a treatment in 5% H_2/Ar atmosphere at 800^{o}C, shown in

Fig. 6(e), reveals the emergence of A_2BO_4 type diffractions in LSCM as well weak diffractions resulting from the ABO_3 type.

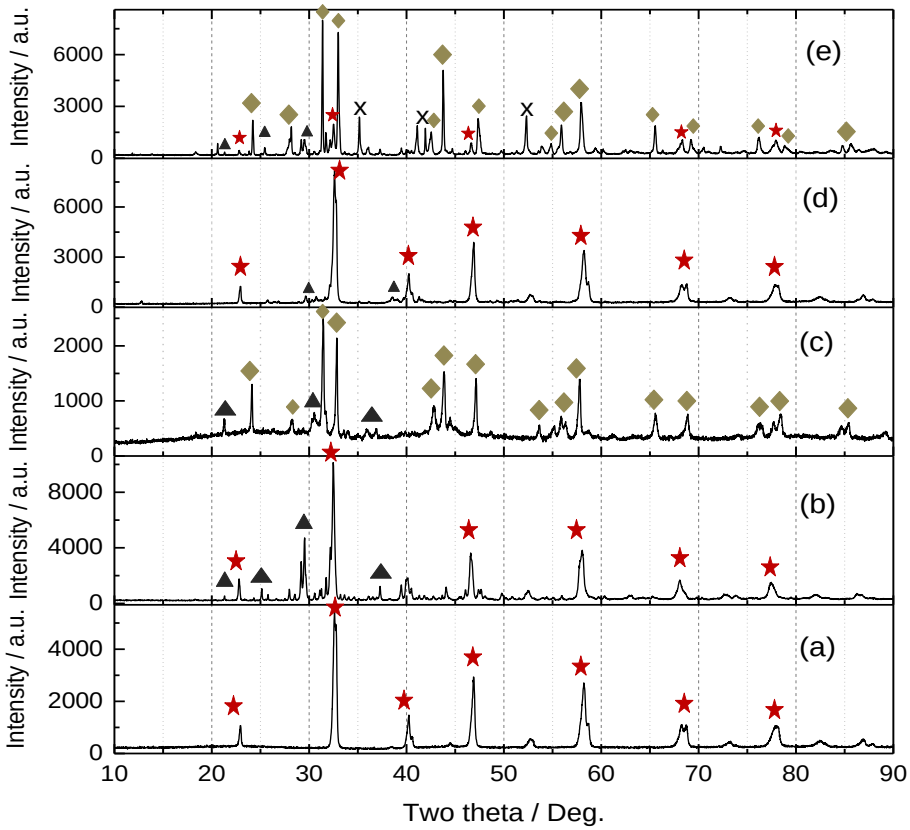

Fig. 6 XRD pattern of LSCM with xerogel and/or carbonate mixture under various treatment conditions. (a) xerogel-LSCM at 800°C in N_2, (b) Li_2CO_3-K_2CO_3- LSCM at 800°C in N_2, (c) xerogel- Li_2CO_3-K_2CO_3-LSCM at 800°C in N_2, (d) xerogel-K_2CO_3-LSCM at 800°C in N_2, and (e) Li_2CO_3-K_2CO_3-LSCM at 800°C in 5% H_2/Ar. The symbols interpolated stand for: Star--ABO_3 perovskite; diamond--A_2BO_4 type oxide; x—unknown phase, possibly MnO; triangle--diffraction peaks from carbonate or Li/K compounds formed during pyrolysis (peaks for Li/K carbonate or compound are not differentiate here for simplicity).

LSCM itself is usually believed to be stable in either reducing or oxidizing atmospheres, which has been frequently applied as promising anode material in H_2/hydrocarbon-fuelled SOFC, though there is a variation from rhombohedral/hexagonal in air to orthorhombic perovskite in H_2 atmosphere [16]. The reduction in perovskite LSCM in Fig. 6 (c and e) can thus be accredited to the interaction/reaction between LSCM and carbonate in reducing atmospheres. It was doubted that this interaction/reaction of LSCM with Li-K carbonate was due to the well-known mobile lithium ions which diffused into the ABO_3 lattice and led to the structure transformation in LSCM. To demonstrate this, a treatment of the mixture without Li_2CO_3, i.e. xerogel-K_2CO_3-LSCM, was carried

out in the same conditions as with Li_2CO_3. The XRD pattern in Fig. 6(d) indicates that no phase change in LSCM occurs after treatment without Li_2CO_3. Clearly, Li attack is the origin for the appearance of A_2BO_4 type oxide in replacement of ABO_3 in LSCM in reducing atmosphere. The interaction/reaction between LSCM and Li_2CO_3 may facilitate the reduction in LSCM besides the reducing power of the carbon form. The perovskite related A_2BO_4 type oxide was reported to have much lower electrical conductivity compared to its ABO_3 counterpart containing the same cations, especially when B=Mn, Fe [24]. A treatment and characterization of GDC with carbon/carbonate mixture powders suggests no phase change in GDC powder in the same conditions as in the case of LSCM.

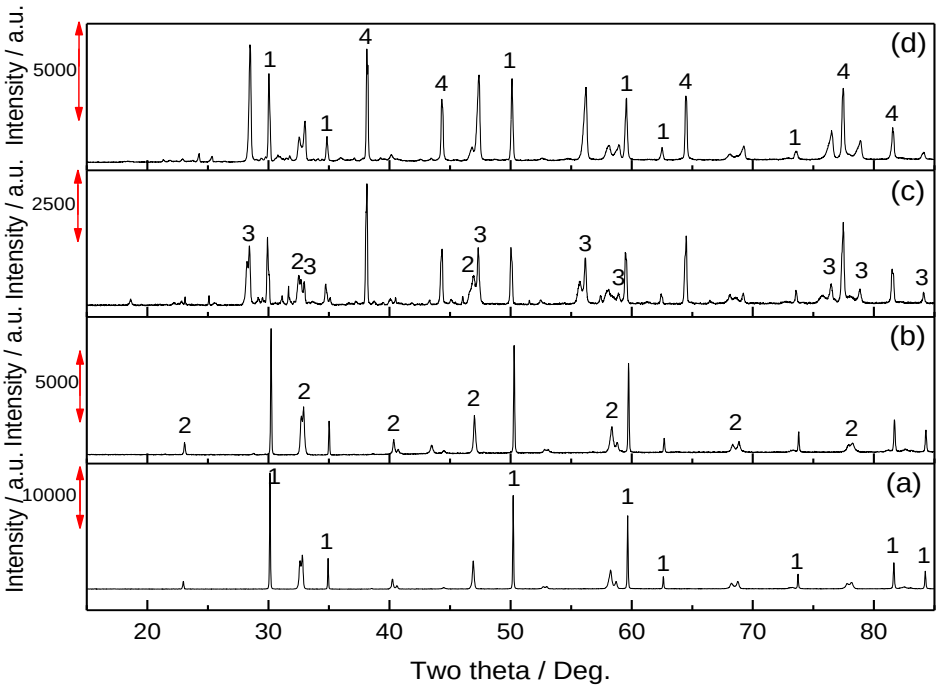

Fig. 7 XRD pattern of (a) fresh LSCM-YSZ pellet, (b) LSCM-YSZ pellet after treatment with Li-K carbonate eutectic in 5% H_2/Ar at 700°C for 10hrs, (c) GDC-LSCM anode after HDCFC operation on xerogel (electrochemical performance shown in Fig. 1 and Fig. 8), and (d) GDC-LSCM anode after DCFC operation on coal (electrochemical performance shown in Fig. 4 and Fig.9-10). Note that diffraction peaks labelled with 1, 2, 3 and 4 stands for YSZ, ABO_3- structured LSCM, GDC, and Ag, respectively.

An additional experiment, involved the treatment of LSCM-YSZ pellet with Li_2CO_3-K_2CO_3 slurry in reducing atmosphere was conducted. The LSCM-YSZ (50-50 in weight ratio) pellet was immersed in Li-K carbonate (Li:K 62:38 in molar ratio), heated to 700°C, and dwelled for 10 hours in 5% H_2/Ar atmosphere. Fig. 7 presents the XRD pattern of a fresh LSCM-YSZ pellet and of the pellet after

treatment. In the fresh pellet, only peaks from ABO_3 perovskite and YSZ are detected, as expected. In the treated LSCM-YSZ pellet, the ABO_3 type perovskite structure is maintained after being exposed to carbonate in 5% H_2/Ar for 10h at 700^{o}C. These observations are obviously on the contrary to that involved LSCM powder. Similarly, the GDC-LSCM anode seems to be stable after HDCFC operation on xerogel and on bituminous coal at 750^{o}C (addressed in section 3.3), as shown in Fig. 7 (c) and (d) respectively, as no significant phase change can be found in LSCM after DCFC operation on either xerogel or raw coal. Apart from weak peaks due to Li_2CO_3 and $KHCO_3$ residuals on the surface of GDC-LSCM anode, diffraction peaks expected from YSZ, GDC, ABO_3-type LSCM and Ag current collector are well assigned in Fig. 7(c-d).

3. 3 Fuel cell durability test and post-mortem characterizations

3.3.1 With xerogel

A short-term HDCFC operation at 750^{o}C at a constant voltage of 0.7V was carried out on xerogel after initial performance evaluation (addressed in section 3.1.1). The current density at 0.7V as a function of time is exhibited in Fig. 8(a). It is seen that the current density sustains at ~50mA cm^{-2} for 1.5hours at the beginning of the potentiostatic operation, probably due to the participation of H_2 and/or CO gases (liberated from xerogel or from gasification reactions) in the anode electrochemical reactions which stabilises the cell performance. After 1.5h, the current density gradually declines and levels off to ~3mA cm^{-2} at the end of the test which lasts for 17hrs in total without interruption in the middle. A decrease in OCV value from 1.12V to 1.06V was noticed before and after the potentiostatic operation. This latter value is close to the equilibrium for carbon oxidation at 750^{o}C, consequently, carbon oxidation seems to be residual process on HDCFC anode, but at a sluggish kinetics. The phenomena mentioned above is supported by the impedance comparison before and after stability test, shown in Fig. 8(b). An extremely large cell resistance is observed after ~17hrs discharge at 0.7V, with both the high frequency arc characterized at 3000Hz and the other one at low frequency zone significantly larger than those before discharge.

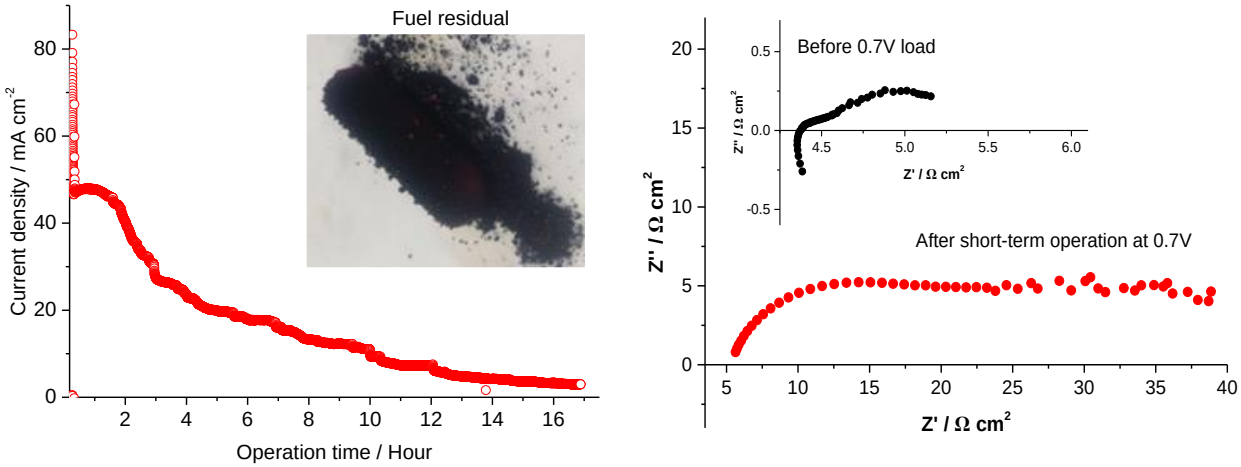

Fig. 8 (a) Current density variations in the short-term HDCFC operation at 0.7V at 750°C on xerogl with the GDC-LSCM oxide as SOFC anode and 2mm thick YSZ pellet as solid electrolyte (the inset in (a) is a picture of residual fuel after fuel cell operation); (b) impedance comparison before and after ~17h HDCFC operation at 0.7V.

Inserted in Fig.8 (a) is a picture of the remaining xerogel-carbonate mixture after DCFC operation, taken when the fuel was poured out from anode chamber at room temperature. Interestingly, the remaining xerogel/carbonate powder ignited spontaneously once exposed to air. The vigorous ignition totally changed the composition and textural properties of the remaining fuel. This process is consistent with the presence of peroxide or super oxide which can act as an oxidant for residual organic matter. Formation of peroxidic species is anticipated in Lux Flood basic system such as these molten carbonates.

3.3.2 with raw bituminous coal (B-II-M)

The durability of a HDCFC with GDC-LSCM oxide anode operating on B-II-M coal was also performed at 0.7V at 750°C for a period of ~70hrs, with the initial cell performance discussed in section 3.1.2. The discharge rate as a function of time during the stability test on raw coal is presented in Fig. 9. One can see from Fig. 9 that the current density at 0.7V (with an initial value of 70mA cm^{-2}) decreases at a relatively low rate in the first 9hrs, it drops quickly afterwards to 15mA cm^{-2} upon reaching 16h. The break after 16h brings back the discharge rate to around 32mA cm^{-2} which maintains the cell for another 15hrs at a low degradation, and afterwards, the current density decays to 10mA cm^{-2} when reaches 40h. The cell performance seems sustained subsequently until reaching 64h, and the discharge rate declines to 5mA cm^{-2} when the durability test was stopped at ~68h.

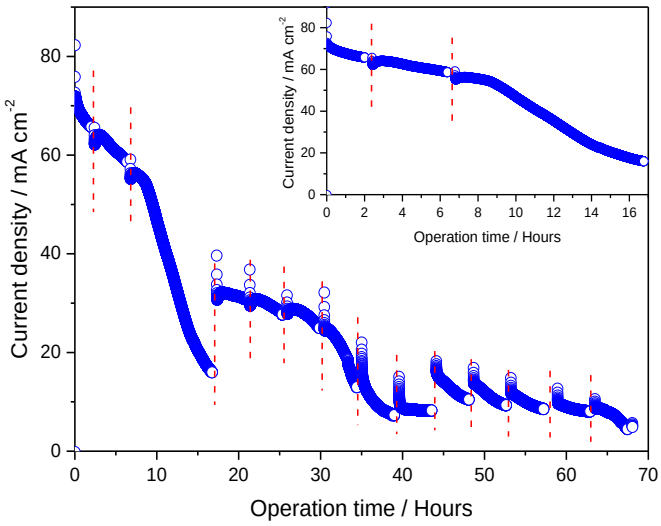

Fig. 9 Current density as a function of operation time for a HDCFC that consists of GDC-LSCM as SOFC anode and a 1mm thick YSZ pellet as solid oxide electrolyte working on B-II-M at 0.7V at 750^{o}C for a period of ~70 hrs.

In Fig. 9, the potentiostatic operation at 0.7V was stopped at each breaking lines for impedance test, and the cell was rested at OCV for 0.5h before impedance measurement. The impedance spectra at each break are displayed in Fig. 10. It is observed from Fig.10 that the cell resistance degrades markedly with operation time, especially after 6hrs. In the first 6hrs, the increases in impedance are relatively small with slightly larger Rs and Rp than the initial values, which can be explained by the involvement of electrochemical oxidation of gaseous H_2/CO released from coal or from facile gasification and oxidation kinetics as a result of low crystallinity in bituminous coal at initial stage. After 6hrs, both Rs and Rp, especially Rp, enlarges significantly due to inadequate production of gaseous fuel and consumption of active carbon in coal. These observations are consistent with the current density variation vs. operation time illustrated in Fig. 9. The impedance results also see an increasingly large high frequency arc characterised at 40000Hz with elongation of operation time, which is absent initially (Fig. 4(b)). Note that after 57hrs, the impedance spectrum features a large high frequency arc with an enormous spike following the high frequency arc, which suggests that the cell suffers from severe mass diffusion resistance. This might result from lack of carbon at the active reaction zone after carbon being consumed or accumulation of mineral matter/alkali metal oxides on the surface of carbon which makes the fuel hardly accessible. Correspondingly, an OCV value of 1.03V in the end of durability test suggests the oxidation of solid carbon being the dominant reaction.

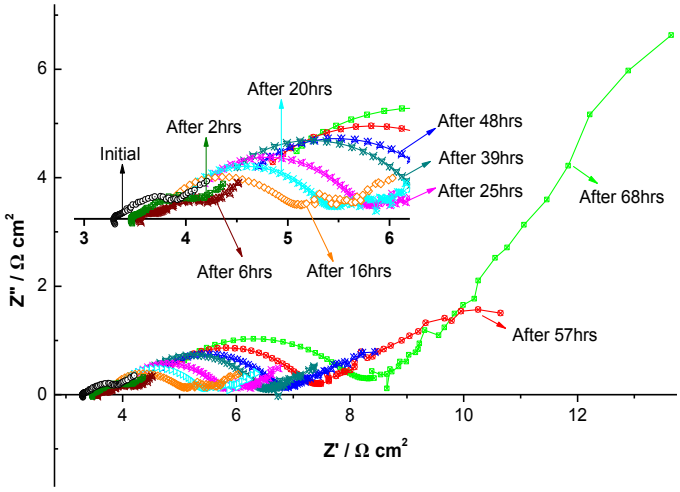

Fig. 10 Impedance evolution of the DCFC with an GDC-LSCM oxide SOFC anode and 1mm thick YSZ solid electrolyte operation on B-II-M coal during stability test at 750°C at 0.7V (the interpolated is a close-up look at the impedance at different time)

The microstructure of the oxide anode after HDCFC operation on coal was examined by SEM incorporated with EDX line-scan, with the result demonstrated in Fig. 11. As expected, Zr and Y are only found in the layer adjacent to the YSZ electrolyte, whereas La and Cr in the outer layer close to the bulk of coal/carbonate mixture and Ce/Gd the whole depth of SOFC anode from EDX. Apart from the above elements, K, sulphur and carbon are seen mainly distributed in the outmost of GDC-LSCM anode. Ag is found only at an area close to LSCM at outside of anode. It is interesting that K, S and C are also seen in the bulk GDC-LSCM anode and area close to dense electrolyte. This originates from a unique phenomenon in bituminous coal, which passed through a plastic stage during heating up to DCFC operational temperature. The coal displayed a fluid-like nature at the plastic stage. This unique characteristic of bituminous coal has been noticed recently in our lab to impact the HDCFC electrochemical performance tremendously, compared to other raw coals and pre-treated coals [25]. The increased fluidity in raw B-II-M coal coupled with melting of eutectic around 490°C in anode chamber bring the coal/carbonate mixture inside the bulk anode of SOFC (as illustrated by EDX), which is beneficial for anode reactions in HDCFC as it extends reaction region and improves further the interactions between SOFC anode and coal once solidified at 650-750°C after passing through its plastic stage. This also explains the reason for the superior electrochemical activity observed on raw B-II-M coal in Fig. 4.

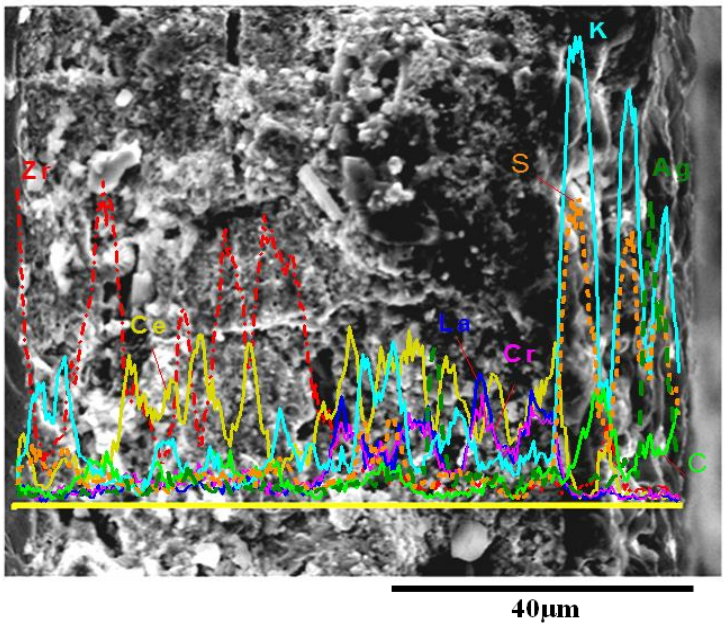

Fig. 11 SEM-EDX result of the GDC-LSCM SOFC anode after ~70h DCFC operation on B-II-M coal at 0.7V at 750^{o}C.

However, the disadvantage is that impurities in raw bituminous coal, e.g., sulphur, quartz and alumina (Table II (b)), were also delivered into the bulk SOFC anode through the plastic stage, which is concerned in its negativity in affecting DCFC long-term performance, as shown in Fig. (9-10). Liu et.al exposed a series of LSCM with different Cr/Mn ratio to 10% H_2S/H_2 at 950^{o}C up to 5 days, and found MnS, La_2O_2S and MnOS impurities on $La_{0.75}Sr_{0.25}Cr_{0.5}Mn_{0.5}O_3$ with decreased conductivities [26]. Although impurity phases were not identified in GDC-LSCM anode after stability test on raw B-II-M coal (Fig. 7(d)) in present study, the presence of S in the bulk SOFC anode may block carbon from accessing O^{2-} for oxidation.

In EDX line-scan, Si and Al are not noticeable, probably due to the low ash content in B-II-M. Nonetheless, the inorganic residuals (in another word, ash) building up in B-II-M/carbonate mixture on the top layer of SOFC anode was visually clear when collecting the remaining fuel after finishing fuel cell testing, because of the appearance of white/light brown particulates. The precipitation of ash from coal and its accumulation with time may form a barrier layer on anode surface, blocking diffusion of reactants to anode active sites for oxidation. Additionally, the carbonate that appears in the matrix of SOFC anode possibly poses the SOFC anode to a harsh condition due to the aggressive nature of carbonate, as evidenced in Fig. 6. The decomposition of carbonate on the other hand, produces extra ash on the surface of coal/SOFC anode. These all could contribute to the increased impedance during DCFC long-term operation, as reflected Fig. 10, resulting in decay of cell performance.

Last but not least, with the ongoing of carbon oxidation at the potentiostatic operation, the coal, loaded at a batch mode for initial characterizations, is subjected to agglomeration and structural changes compared to fresh coal. In Fig. 5, the (002) reflection at $2\theta = 25.2^{o}$ is hardly visible in the remaining coal after DCFC durability test, which is reasonable as most of H_2 releasing groups and active carbon sites were probably used up leading to an ordered structure in the remaining coal. Accompanied with the consumption of carbon inside the SOFC anode and those near the interface of SOFC anode and coal/carbonate mixture, oxidation of coal in the bulk of coal/carbonate mixture may become difficult due to mass diffusion problems, which possibly interprets the enormous spike appeared on impedance spectra after 60hrs in HDCFC durability test. To develop a practical system, operation based on continuous feeding is essential to keep up high power output. Future work on HDCFC operation with a refuelling design may be conducted using a gravity based feeding tube with an auger to deliver carbon/carbonate mixture into anode chamber to address this issue in practical HDCFC application.

As mentioned in previous section, the reaction between LSCM and carbonate leading to the formation of perovskite-related A_2BO_4 oxide was not observable after fuel cell durability test on either xerogel or raw coal. The ABO_3 structure was generally retained in LSCM after HDCFC durability operation, as illustrated in the XRD pattern in Fig. 7(c-d). The contrast in the stability of LSCM powder and GDC-LSCM anode with carbonate is associated with difference in contacts between perovskite and carbonate. LSCM is susceptible to lithium carbonate attack within intimate contacts between LSCM powder and carbonate in pyrolysis experiment (Fig. 6(c-e)), whereas in GDC-LSCM anode, it is possible that the impregnation of GDC fine particles protect LSCM from Li attack, thus enhances LSCM-containing anode stability. However, longer-term tests, incorporated with operation based on continuous fuel top-up, are needed to confirm or disprove this and to address as well the possibilities of sulphur poisoning especially when coal is used.

4. Conclusions

In this work, attempt of applying oxide materials such as $(La,Sr)(Cr,Mn)O_3$ (LSCM) and $(Gd,Ce)O_2$ (GDC) in hybrid direct carbon fuel cells was made, with the electrochemical performance of HDCFC with the GDC-LSCM oxide anode (prepared by wet impregnation) evaluated on batch mode loading of two solid fuels, an organic xerogel and a raw bituminous coal. The SOFC with infiltrated oxide anode was sealed to an alumina tube, which was loaded with carbon/Li-K carbonates mixture afterwards, acting as HDCFC anode. DC polarization curves and ac-impedance spectroscopy were measured at 650-800^{o}C with N_2 as purge gas in anode. The HDCFC with oxide anode showed a

notably higher performance than that with the traditional Ni-YSZ anode on xerogel as a result of high conductivity as well as high electro-catalytic properties offered by GDC-LSCM oxide derived from wet impregnation fabrication. High OCV values, in the range of 1.1-1.2V, and low total Rp values (0.8-0.9 Ω cm^2) at 750^{o}C were reached on HDCFC with oxide anode running on both xerogel and a bituminous coal with ash and sulphur impurities. These suggest the potential application of this GDC-LSCM oxide material in HDCFC operating with different carbon forms.

The compatibility of LSCM/GDC with carbon/carbonate mixture was investigated at 700-800^{o}C in various conditions. It was found that an interaction/reaction between LSCM and lithium carbonate in reducing environment facilitated the reduction in ABO_3-type perovskite LSCM, leading to the formation of perovskite-related A_2BO_4 oxide as a result of the intimate contact between LSCM and carbonate. The GDC remained its original structure under identical conditions. However, the above phenomenon in LSCM was not detectable on the LSCM-YSZ pellet treated with carbonate in reducing atmosphere at 700^{o}C for 10hrs, nor on the GDC-LSCM oxide anode after HDCFC operation at 0.7V at 750^{o}C on xerogel as well as on the raw bituminous coal.

Degradation regarding the HDCFC durability test on xerogel at 0.7V at 750^{o}C with a period of ~17hrs was mainly due to the loss of carbonate, which generated some active species that ignited spontaneously after exposing the remaining fuel to air at room temperature. The degradation mechanism on raw bituminous coal in a ~70hrs durability test was more complicated, not only because of the existence of ash and sulphur impurities, but also the unique plastic stage raw bituminous coal passed through upon heating up. Factors impacted the performance decay included sulphur poisoning and accumulation of mineral contents/oxide decomposed from carbonate, the occurrence of which was extended in the bulk GDC-LSCM anode as a result of bituminous coal passing a plastic stage. Other factors that were accounted for degradation as well included agglomeration and structural change in coal accompanied by use-up of active carbon in single feed with operation time. In future work, operations of HDCFC with GDC-LSCM oxide anode in a longer-term, coupling with continuous fuel feeding, will be required to address the practical application of this anode material in DCFCs, especially those running on coal.

Acknowledgements

The authors would like to thank the European project 'Efficient conversion of coal to electricity-Direct Coal Fuel Cells', funded by the Research Fund for Coal & Steel (RFC-PR-10007), and also thank Dr. Aida Fuente Custa for her kind help on gathering the results on properties analysis of carbon and coal.

References

1. T. M. Gür, *Chem. Rev.*, 2013, **113**, 6179.
2. S. Giddey, S. P. S. Badwal, A. Kullkarni, C. Munnings, *Prog. Energy Combust.*, 2012, **38**, 360.
3. N. J. Cherepy, R. Krueger, K. J. Fiet, A. F. Jankowski, and J. F. Cooper, *J. Electrochem. Soc.*, 2005, **152**, A80.
4. X. Li, Z. Zhu, R. De Marco, A. Dicks, J. Bradley, S. Liu, and G. Lu, *Ind. Eng. Chem. Res.*, 2008, **47**, 9670.
5. X. Li, Z. Zhu, R. De Marco, A. Dicks, *J. Power Sources*, 2010, **195**, 4051.
6. G. A. Hackett, J. W. Zondlo, R. Svensson, *J. Power Sources*, 2007, **168**, 111.
7. X. Zhou, T. Oh, J. M. Vohs, and R. J. Gorte, *J. Electrochem. Soc.*, 2015, **162**, F567.
8. F. Lantelme and H. Groult, Molten Salts Chemistry; Elsevier Inc., 2013, Chapter 19, pp403.
9. S. L. Jain, J. B. Lakeman, K. D. Pointion, J. T. S. Irvine, *J. Fuel Cell Sci. Tech.*, 2007, **4**, 281.
10. Y. Nabae, K. D. Pointon and J. T. S. Irvine, *Energy Environ. Sci.*, 2008, **1**, 148.
11. S. L. Jain, J. B. Lakeman, K. D. Pointion, R. Marshall, and J. T. S. Irvine, *Energy Environ. Sci.*, 2009, **2**, 687.
12. C. Jiang, J. Ma, A. D. Bonaccorso, and J. T. S. Irvine, *Energy Environ. Sci.*, 2012, **5**, 6973.
13. A. C. Chien, A. Arenillas, C. Jiang, and J. T. S. Irvine, *J. Electrochem. Soc.*, 2014, **161**, F588.
14. S. P. Jiang, S. H. Chan, *J. Mater. Sci.*, 2004, **39**, 4405.
15. S. Tao and J. T. S. Irvine, *Nat. Ma*t., 2003, **2**, 320.
16. S. Tao and J. T. S. Irvine, *J. Electrochem. Soc.*, 2004, **151**, A252.
17. U. Hennings, R. Reimert, *Appl. Catal. A: General*, 2007, **325**, 41.
18. R. D. Green, C. C. Liu, S. B. Adler, *Solid State Ionics*, 2008, **179**, 647.
19. X. Yue, and J. T. S. Irvine, *ECS Trans.*, 2015, **68**, 3535.
20. L. Zubizarreta, A. Arenillas, J. Piard, J. Pis, N. Job, *Micropor. Mesopor. Mat.*, 2008, **115**, 480.
21. N. Job, R. Pirard, J. Marien, J. Pirard, *Carbon*, 2004, **42**, 619.
22. M. M. Rahman, Nanomaterials; InTech, 2011, Chapter 9, pp187.
23. K. Chen, N. Ai, and S. Jiang, *J. Electrochem. Soc.*, 2010, **157**, P89.
24. M. Al Daroukh, V. V. Vashook, H. Ullmann, F. Tietz, I. A. Raj, *Solid State Ionics*, 2003, **158**, 141.
25. A. Fuente-Cuesta, C. Jiang, A. Arenillas, J. T. S. Irvine, *Energy Environ. Sci.*, 2015, submitted.
26. S. Zha, P. Tsang, Z. Cheng, M. Liu, *J. Solid State Chem.*, 2005, **178**, 1844.